Appl. Phys. B 72, 151–155 (2001) / Digital Object Identifier (DOI) 10.1007/s003400000430

Applied Physics B
Lasers
and Optics

Characterization of optically excited terahertz radiation from arsenic-ion-implanted GaAs

G.-R. Lin[1], **C.-L. Pan**[2]

[1] Institute of Electro-Optical Engineering, Tatung University, 40 Chung Shan North Rd., Sect. 3, Taipei, Taiwan 10451, R.O.C.
(Fax: +886-2/2586-1939, E-mail: grlin@ttu.edu.tw)
[2] Institute of Electro-Optic Engineering, National Chiao Tung University, 1001 Ta-Hsueh Rd., Hsinchu, Taiwan 30010, R.O.C.

Received: 24 August 1999/Final version: 4 July 2000/Published online: 8 November 2000 – © Springer-Verlag 2000

Abstract. This work characterizes the optically excited terahertz (THz) radiation from arsenic-ion-implanted GaAs (GaAs : As^+). We observed phase reversal in the emitted THz radiation field after the semi-insulating GaAs substrate was implanted. The peak amplitude of the emitted THz field increased from 25 mV/cm to 100 mV/cm after thermal annealing. This trend confirms the recovery in crystallinity of the as-implanted GaAs : As^+ after annealing. By introducing a magnetic field, we observe a blue shift of the center frequency in the THz power spectrum from 0.57 THz for the as-implanted GaAs : As^+ to 1 THz for furnace-annealed samples. Analysis of the blue-shifted spectra and unsymmetrical pulse shapes allows us to infer the increasing importance of the contribution of another unknown mechanism to the THz radiation from the GaAs : As^+ samples after annealing. This is also explained satisfactorily by the crystallinity of the as-implanted and furnace-annealed GaAs : As^+. Further, the effective carrier mobilities of as-implanted, rapid-thermal-annealed, and furnace-annealed GaAs : As^+ are determined for the first time as 0.6, 2, and 15 cm^2/Vs respectively according to the THz data.

PACS: 78.47.+p; 61.72.Vv; 72.20.Jv; 73.30.+y; 42.88.+h; 42.50.Md; 42.65.Ky

---

Terahertz (THz) radiation systems have received extensive interest owing to their widespread scientific and military applications. The ultra-wide-band and quasi-optical characteristics also account for the substantial efforts made to apply THz technology for spectrally determining the dielectric parameters of crystals, polymers, and organic liquids, etc. Recently, optically excited THz radiation (OETR) from an unbiased semiconductor surface [1, 2] has also been investigated. The OETR was subsequently employed as a novel optoelectronic technique for characterizing the electrical and optical parameters of semiconductors. However, few experiments [3, 4] have been demonstrated to realize the effect of physical/chemical processes on the characteristics of the semiconductor surfaces or depletion layers. Shen et al. [4] reported the effect of nitrogen-ion implantation on GaAs by characterizing the time-resolved reflectivity and OETR. More recently, the ultrafast carrier dynamics of the arsenic-rich GaAs grown by low-temperature molecular-beam epitaxy (referred to as LT-GaAs) have also been studied via THz spectroscopy [5]. On the other hand, the arsenic-implanted GaAs (GaAs : As^+) material [6], which possesses very similar properties as the LT-GaAs layer, has emerged as an alternative for ultrafast optoelectronic applications [7–9]. In this letter, we present the first measurement of OETR from as-implanted and post-annealed GaAs : As^+ samples. The effects of thermal annealing time on the carrier lifetimes, effective carrier mobilities, as well as the dominating radiating mechanisms of the GaAs : As^+ material have also been primarily demonstrated.

The GaAs : As^+ samples were prepared by implanting the liquid-encapsulated-Czochralsky (LEC)-grown, (100)-oriented, semi-insulating (S.I.) GaAs substrate with 200 keV arsenic ions at a dosage of 10×10^{16} ions/cm^2 in a commercial apparatus (Varian E220). The encapsulated, ex-situ annealing process was performed at 600 °C in either a rapid-thermal-annealing (RTA) processor for 30 s or a quartz-tube furnace for 30 min with flowing nitrogen gas. For detection of OETR, we employed the electro-optic field-sensing technique that has been demonstrated by Wu and Zhang [10]. A 1.5-mm thick, (110)-oriented ZnTe crystal was used as the THz field sensor. The light source was a mode-locked Ti:sapphire laser (Spectra-Physics, Tsunami, $\lambda = 0.8\,\mu m$) which generates 130-fs optical pulses at a repetition rate of 82 MHz. The average powers of the optical pump and probe beams were about 1 W and 150 μW, respectively. The spot size of the unfocused pump beam was about $3 \sim 4$ mm. A pellicle beamsplitter that is 90% transparent for the THz beam was used to collimate the focused probe beam along the propagation direction of the THz beam. For some of the experiments, the arsenic-ion-implanted GaAs samples were further subjected to an external magnetic field (~ 0.32 T) which is perpendicular to the direction of the optical axis.

For the first OETR experiment, the sample was positioned with its surface normal tilted from the propa-

gating direction of the pump beam at an angle of about $65 \sim 70°$ [11]. This arrangement facilitates the radiated field strength along the optical axis. The OETR patterns from as-implanted, RTA-annealed, and furnace-annealed $GaAs:As^+$ samples are displayed in Fig. 1. The corresponding positive and negative peak photocurrents are $I_{positive} = 0.47$ ($I_{negative} = -0.53$) nA, 0.78 (−0.71) nA, and 1.82 (−2.21) nA for the above three types of samples, respectively. The corresponding THz field strength, E_{rad}, can be expressed as $E_{rad} \cong I_{ph}/(1.2 \times 10^{-6} \cdot P_{in})$ V/m by using the e lectro-optic coefficients of the ZnTe crystal and Jones matrices, where I_{ph} and P_{in} are the photocurrent detected by the lock-in amplifier and the reflected power of the optical probe beam, respectively. Note that the THz field discussed in our case is only the internal field inside the ZnTe probe crystal. The external THz field is not considered due to the lack of the refractivity data of the $GaAs:As^+$ sample at such wavelength. Our results indicate that $E_{rad} \approx 25\,(-30)$ mV/cm, 48 (−38) mV/cm, and 100 (−124) mV/cm for as-implanted, RTA-annealed, and furnace-annealed $GaAs:As^+$, respectively. In comparison, the THz radiation from unbiased S.I. GaAs exhibits larger negative and positive peak currents of about −3.3 nA and 9.2 nA. These correspond to peak radiated field strengths of −190 mV/cm and 520 mV/cm, respectively. In addition, we further observed that the phases of the radiated THz signals from all the $GaAs:As^+$ samples are reversed from that of S.I. GaAs (see Fig. 1). Previously, this phenomenon has also been observed in either Si semiconductors (with $p-i-n$ and $n-i-p$ type structures) [3] or nitrogen-ion-implanted GaAs substrates [4]. These investigations explained such a phenomenon as the field reversal near a semiconductor surface. In view of the aforementioned works, we therefore infer that the phase-reversed THz radiation from the $GaAs:As^+$ samples is caused by the reversal of the direction of the surface depletion field. The dense As antisite defects generated by the ion-implantation process are thought to be responsible for this phenomenon, which leads to a strong Fermi-level pinning effect on the surface of the heavily implanted $GaAs:As^+$ samples. It is worth noting that the density of the As_{Ga} antisite defects, $N[As_{Ga}]$, in the as-implanted (non-annealed) $GaAs:As^+$ sample is up to $1.5 \times 10^{20}\,cm^{-3}$. $N[As_{Ga}]$ only decreases to be an order of magnitude smaller even for a high-temperature RTA-annealing process. After a long-term furnace-annealing process, $N[As_{Ga}]$ in the $GaAs:As^+$ sample is found to be $2 \sim 5 \times 10^{18}\,cm^{-3}$. Such an amount of defects can only be found in heavily doped semiconductors. We therefore conclude from these observations that the un-implanted S.I. GaAs substrate is slightly p-type, and thus all of the implanted samples (annealed and non-annealed ones) should have been transformed to n-type.

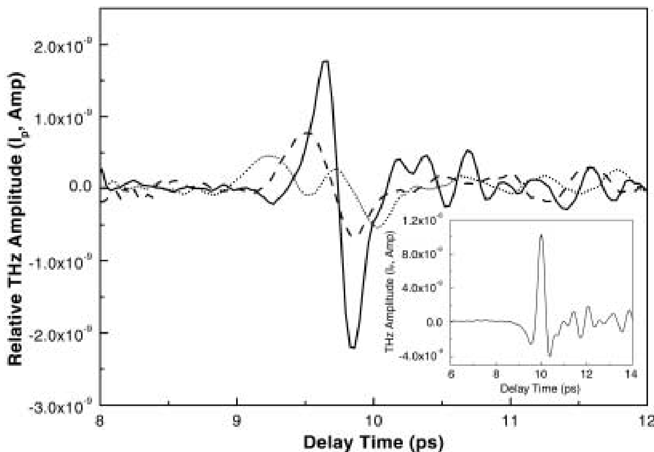

Fig. 1. The THz radiation pattern of as-implanted *(short-dotted line)*, RTA-annealed *(dashed line)*, and furnace-annealed *(solid line)* $GaAs:As^+$ samples. The *inset figure* illustrates the THz radiation from the S.I. GaAs sample

Furthermore, according to our results, the THz field strength increases as the annealing time lengthens. The current-surge mechanism suggests that either the increasing carrier mobility, or the enhanced surface depletion field, or the lengthening carrier lifetime can essentially enlarge the strength of the radiated THz field. According to the Hertzian dipole radiation model that predominates the current-surge mechanism, the field strength of THz radiation can be written as

$$E_{rad}(t) \propto \frac{\partial J_{ph}(t)}{\partial t} = qn_{ph}\frac{\partial V_d}{\partial t} + qV_d\frac{\partial n_{ph}}{\partial t}$$
$$\propto q\mu_{eff}E_{surface}n_{ph}(t)/\tau_{ph}, \quad \text{when } t \geq 0$$

where V_d denotes the drift velocity of photoexcited carriers, $n_{ph}(t) \approx n_0\,e^{-t/\tau_{ph}}$ is the transient photoexcited carrier density, μ_{eff} is the effective carrier mobility of the sample, $E_{surface}$ is the surface depletion field near the semiconductor surface, and τ_{ph} is the photoexcited carrier lifetime. This approximation is sustained if we consider that the width of the laser pulse is far shorter than the lifetime of the photoexcited carriers and the duration of the excited THz pulse. The effective carrier mobility of the $GaAs:As^+$ materials thus can be estimated owing to the aforementioned relationship at $t = 0$. Previously, our electrical measurements revealed that the magnitudes of the barrier height ψ_S (as well as the surface field) at the surface of as-implanted and RTA-annealed $GaAs:As^+$ samples were about 0.49 and 0.55 eV, respectively. After a long-term annealing, ψ_S of the furnace-annealed $GaAs:As^+$ further increases to $0.57 \sim 0.6$ eV [12]. Since the measured surface potentials are very close to the activation energy of the arsenic antisite defect in the $GaAs:As^+$ sample [13], it is reasonable to postulate that the Fermi-level pinning effect caused by the dense antisite defects should exist in the as-implanted and annealed $GaAs:As^+$ samples. In comparison, these values are relatively comparable with that of S.I. GaAs (~ 0.75 eV). The width and field of the depletion region at the $GaAs:As^+$ / S.I. GaAs interface can be expressed as

$$d_{total} = \sqrt{\frac{2\,\varepsilon V_{bi}}{q}\left[\frac{N_{SI}+N_{As}}{N_{SI}N_{As}}\right]} \approx \sqrt{\frac{2\,\varepsilon V_{bi}}{qN_{SI}}}$$
$$E_{max} = \frac{qN_{SI}d_{SI}}{\varepsilon} = \frac{qN_{As}d_{As}}{\varepsilon} \approx \frac{qN_{SI}d_{total}}{\varepsilon} \approx \sqrt{\frac{2qN_{SI}V_{bi}}{\varepsilon}},$$

where d_{total} is the depletion width, E_{max} is the depletion field, V_{bi} is the built-in potential, ε is the relative permittivity (i.e., dielectric constant), and N_{SI} and N_{As} are the dopant concentrations in the bulk and implanted regions. The depletion width at the bulk S.I. GaAs side is calculated with $N_{SI} < 5 \times 10^7\,cm^{-3}$ [14], which approximately

Table 1. The related key-parameters of the S.I. GaAs and GaAs:As^+ samples

Sample	THz fields / mV/cm	Lifetime / ps	Barrier height / eV	Surface field / V/cm	Mobility / cm^2/Vs
GaAs : As^+, As-imp.	25	0, 26 ∼ 0.28	0.49	2.61	0.63 (1)
GaAs : As^+, RTA	48	0.45	0.55	2.75	1.9 (3)
GaAs : As^+, Furnace	100	1.6 ∼ 1.9	0.57 ∼ 0.6	2.88	15.1 (24)
S.I. GaAs	−190	350	−0.75	3.22	5000 (8000)

equals the total depletion width since the depletion depth toward the heavily implanted GaAs region is negligibly small. Therefore, the depletion width is relatively large in the bulk S.I. GaAs region due to the ultra-low dopant concentration of the S.I. GaAs substrate. The total depletion width and surface field of each sample were also calculated by using the aforementioned equations, as shown in Table 1.

The time-resolved reflectivity measurements indicate that the lifetime for photoexcited carriers in the GaAs : As^+ samples ranges from 0.26 ∼ 0.28 ps for the as-implanted sample, slightly increases to 0.45 ps in a RTA system for 30 s, and further lengthens up to 1.8 ps after long-term annealing for 30 min [9]. These are shown in Fig. 2. Based on these experimental data, the ratios of carrier mobilities for as-implanted, RTA-annealed, furnace-annealed GaAs : As^+ and S.I. GaAs are thus determined to be 1 : 3 : 24 : 8000. If we consider that the carrier mobility of a commercial S.I. GaAs wafer is about 5000 cm^2/Vs, the effective carrier mobilities of as-implanted, RTA-annealed, and furnace-annealed GaAs : As^+ samples are therefore calculated to be about 0.6, 2, and 15 cm^2/Vs, respectively. The corresponding parameters of different samples required for the calculation of the effective carrier mobility are listed in Table 1. The estimated μ_{eff}'s of GaAs : As^+ samples are not only in good agreement with that of other ion-implanted GaAs samples, but also comparable to that of LT-GaAs under the same annealing conditions. Instead of using a conventional Hall measurement under an ultrahigh magnetic field, this is the first measurement of the carrier mobility in ion-implanted, highly resistive semiconductors with such low mobility by using OETR. Moreover, we also note that determining carrier mobility via OETR is completely non-invasive; no electrode has to be fabricated on the sample.

For the second OETR experiment, the unbiased GaAs : As^+ sample was oriented with its surface normal parallel to the propagating direction of the pump beam. In this case, the electron–hole pairs were forced to separate and generate Hertzian dipoles with orientation parallel to the optical axis of the pump beam. The maximum field strength of the radiated THz pulses is located in the direction perpendicular to the optical axis. Notably, the contribution of the current-surge effect to the THz radiation along the propagating direction is nearly negligible in this case. However, by introducing a magnetic field which creates an induced

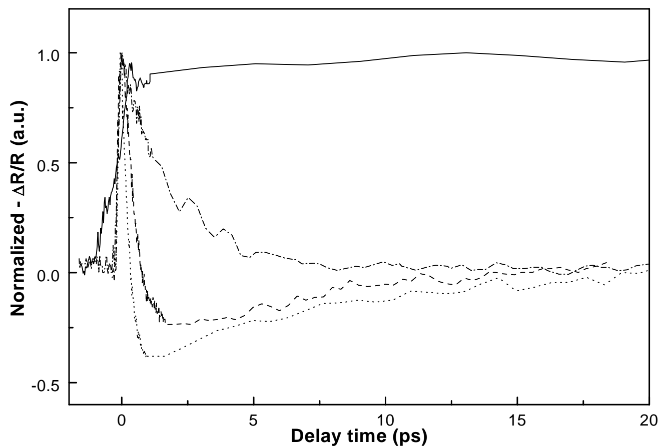

Fig. 2. The time-resolved reflectivities of as-implanted *(short-dotted line)*, RTA-annealed *(dashed line)*, furnace-annealed *(dash-dotted line)* GaAs : As^+, and S.I. GaAs *(solid line)* samples

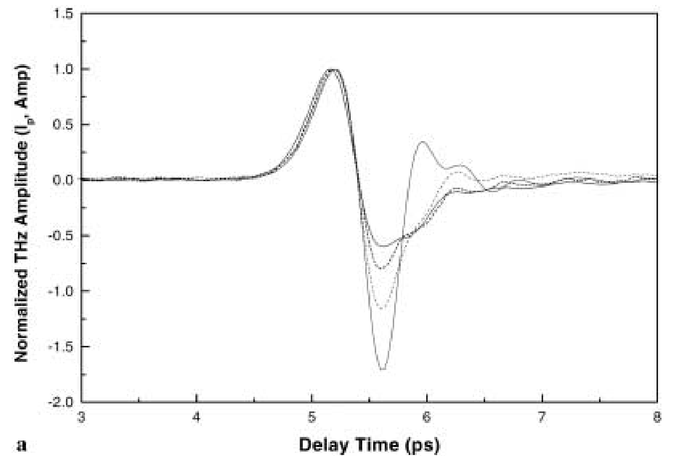

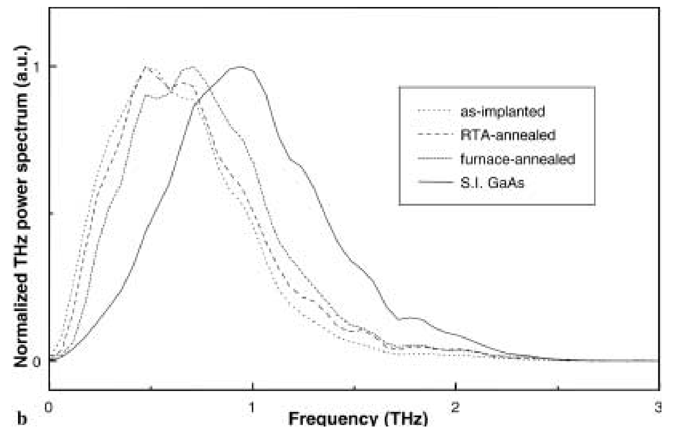

Fig. 3. a Enhancement of THz radiation from as-implanted *(short-dotted line)*, RTA-annealed *(short-dashed line)*, furnace-annealed *(dashed line)* GaAs : As^+, and S.I. GaAs *(solid line)* samples by introducing a magnetic field. **b** The power spectra of THz radiation from different GaAs : As^+ samples obtained by fast Fourier transformation of the time-resolved THz radiation patterns

electric field perpendicular to the surface normal, the photoexcited electron–hole pairs can be separated under this field and generate the transient Hertzian dipoles that are oriented orthogonal to the optical axis. This enhances the strength of THz radiation along the optical axis. The THz radiation from GaAs : As^+ samples under a magnetic field is shown in Fig. 3a. It is found that the peak amplitude of the negative part of the THz radiation increases with an increase of the annealing time. In general, the trend of increasing signal after thermal annealing can be attributed to either the recovery of crystallinity accompanied with the rise of carrier mobility, or the shortening of the carrier lifetime after the annealing process. Since the latter explanation has been ruled out by using the carrier-lifetime data from the femtosecond pump/probe measurements, the experimental results therefore reconfirm our evaluation on the trend of carrier mobilities for the post-annealed GaAs : As^+ samples. Furthermore, we found that these THz radiation patterns can be adequately fitted by the 1st derivative of an auto-correlated hyperbolic secant function convoluted with an exponential decay function, which represents the reduction of carriers in semiconductors during recombination or trapping processes. Especially, the rising part of the measured THz radiation waveforms from different GaAs : As^+ samples matches accurately that of our fitted function without any deviations. These observations indicate that the radiation mechanism for the GaAs : As^+ samples under a magnetic field is likely predominated by the enhanced current-surge effect. However, we also found in the furnace-annealed GaAs : As^+ sample that the negative peak of the normalized THz radiation pattern was found to be slightly larger than the positive peak. A 2nd derivative of the autocorrelated laser-pulse function (of an auto-correlated hyperbolic secant function) has to be introduced for best fitting of the THz radiation of this sample. Although this result cannot be quantitatively explained at present, it may be taken as indirect evidence for the existence of the other mechanism in addition to the current-surge effect.

By performing fast Fourier transformation (FFT) analysis, the center frequencies of the THz power spectra for the GaAs : As^+ samples were determined to range from 0.57 THz to 0.7 THz. In addition, it is found that the full width at half maximum (FWHM) of the THz power spectra for all the GaAs : As^+ samples was about 0.8 THz, which is independent of annealing time (see Fig. 3b). In comparison, the corresponding values for S.I. GaAs are 1 THz and 0.83 THz, respectively. Note that a trend of blue shift in center frequency of THz radiation from GaAs : As^+ annealed at a longer duration was observed in the plot of THz power spectra. Nevertheless, the FWHMs of the THz spectra from all samples still remain constant. According to the theoretical models of THz radiation, it is understood that the THz waveforms can exhibit similar shapes to the 1st-order and 2nd-order derivatives of the correlated laser pulses, respectively. If we assume that the THz radiation is purely excited by either the 1st-order or the 2nd-order derivative of an auto-correlated hyperbolic-secant-shaped optical pulse, the THz power spectrum of the 2nd-order-derivative dominated THz radiation is observed to exhibit a higher center frequency than that of the 1st-order-derivative dominated one. In view of the theoretical simulations and our experimental results, we note that there are two significant features corresponding to the THz radiation waveforms; such features are mainly caused by the combined effect of the 1st-order and 2nd-order derivative components. That is, not only the negative peak can be larger than the positive peak of the THz waveform in the time domain, but also the blue shift of the power spectrum is found in the frequency domain. The semiconductor response (usually an exponential decay function) involved in the photocurrent via a convolution procedure will essentially degrade the ultrafast dynamical response of the original 1st-derivative function by attenuating the amplitude of the negative peak and lengthening the tail of the radiating waveform. This interprets that the center frequency of the THz spectrum induced by the current-surge effect (1st-derivative-function-like pattern) should be slighter lower than that induced by the 2nd-derivative-function-dependent effects. We can also conclude that a small fraction of the THz signal contributed by the 2nd-derivative-function-dependent effects will efficiently lead to a THz power spectrum with higher center frequency. Furthermore, the experimental results for the GaAs : As^+ samples imply that the contributing factor of such effects is enhanced as the annealing time increases. Although we are unable to confirm this, these results still suggest that the orientation of the GaAs substrates after the implantation and annealing processes could have been slightly modified and deviated from the $\langle 100 \rangle$ direction.

In conclusion, this work characterizes the OETR from unbiased, arsenic-ion-implanted GaAs samples. A phenomenon of phase-reversal in the THz radiation field is observed in the GaAs : As^+ samples, in contrast to that in a S.I. GaAs substrate. The field strengths of the as-implanted, RTA-annealed, and furnace-annealed GaAs : As^+ are estimated to be about 25 (−30) mV/cm, 48 (−38) mV/cm, and 100 (−124) mV/cm, respectively. The ratios of effective carrier mobilities of as-implanted, RTA-annealed, furnace-annealed, and S.I. GaAs are primarily evaluated to be 1 : 3 : 24 : 8000 (0.6 : 2 : 15 : 5000 cm^2/Vs) in our work. To date, these are hitherto the preliminary data estimated by OETR rather than by Hall-measurement or photoconductive methods. The experimental data also confirm that the increasing THz field strength is attributed to the recovery of mobility or surface nonlinearity after the thermal annealing process. Under a magnetic field, the current-surge effect is significantly enhanced. The investigations also indicate that either the enhancement of surface electric field or the recovery of carrier mobility would be more pronounced than the shortening of carrier lifetime for the improvement of THz field strength. It is also found that the current-surge effect in the GaAs : As^+ samples could significantly be enhanced during an ex-situ annealing process. The experimental observation on blue shift of center frequency in the THz power spectrum after long-term annealing is elucidated as a contribution of an unknown surface effect that results in a 2nd-derivative-function-like THz waveform. Our simulations also suggest the existence of another radiating mechanism different from the current-surge effect that corroborates with the THz radiation from the implanted GaAs : As^+ samples, which may serve as a less-predominated mechanism in the GaAs : As^+ samples.

Acknowledgements. This work was supported in part by the National Science Council of the Republic of China under various grants. The experimental data was taken at the Rensselare Polytechnic Institute. Comments by Prof. X.-C. Zhang and assistance by Dr. Q. Wu are gratefully acknowledged.

References

1. X.-C. Zhang, B.B. Hu, J.T. Darrow, D.H. Auston: Appl. Phys. Lett. **56**, 1013 (1990)
2. S.-L. Chuang, S. Schmitt-Rink, B.I. Greene, P.N. Saeta, A.F.J. Levi: Phys. Rev. Lett. **68**, 102 (1992)
3. X.-C. Zhang, Y. Jin, L.E. Kingsley, M. Weiner: Appl. Phys. Lett. **62**, 2477 (1993)
4. H. Shen, Y. Jin, G.A. Wagoner, X.-C. Zhang, L. Kingsley: *Ultrafast Phenomena IX*, Springer Series in Chemical Physics 60 (Springer, Berlin, Heidelberg 1994) p. 372
5. S.S. Prabhu, S.E. Ralph, M.R. Melloch, E.S. Harmon: Appl. Phys. Lett. **70**, 2419 (1997)
6. A. Claverie, F. Namavar, Z. Liliental-Weber: Appl. Phys. Lett. **62**, 1271 (1993)
7. H.H. Wang, J.F. Whittaker, H. Fujioka, Z. Liliental-Weber: In *Ultrafast Electronics and Optoelectronics*, OSA Technical Digest Series 13 (OSA, Washington DC 1995) p. 32
8. F. Ganikhanov, G.-R. Lin, W.-C. Chen, C.-S. Chang, C.-L. Pan: Appl. Phys. Lett. **67**, 3465 (1995)
9. G.-R. Lin, W.-C. Chen, F. Ganikhanov, C.-S. Chang, C.-L. Pan: Appl. Phys. Lett. **69**, 996 (1996)
10. Q. Wu, X.-C. Zhang: Appl. Phys. Lett. **68**, 1604 (1996)
11. M. Li, F.G. Sun, G.A. Wagoner, M. Alexander, X.-C. Zhang: Appl. Phys. Lett. **67**, 25 (1995)
12. W.-C. Chen, C.-S. Chang: J. Appl. Phys. **80**, 1600 (1996)
13. G.-R. Lin, W.-C. Chen, C.-S. Chang, C.-L. Pan: Appl. Phys. Lett. **65**, 3272 (1994)
14. D.C. Look: *Electrical Characterization of* GaAs *Materials and Devices* (Wiley, New York 1989) Chapt. 1 pp. 45–47